Interdisciplinary Research in Medical Sciences Specialty
ISSN: 3062-4401
2023, Volume 3, Issue 1, Page No: 146-163

Available online at: www.galaxypub.co/page/journals

Galaxy Publication

A Comparative Evaluation of Colonic Microflora Profiles and Plasma Metabolites in Unilateral Ureteral Obstruction–Related Chronic Kidney Disease Following Intervention with the Chinese Medicine FuZhengHuaYuJiangZhuTongLuo versus AST-120

Mohammed Rahman[1], Abdul Karim[1], Hasan Mahmud[1]*

[1]Department of Clinical Medicine, Faculty of Medicine, University of Dhaka, Dhaka, Bangladesh.

***E-mail** ✉ hasan.mahmud.med@gmail.com

Received: 17 March 2023; **Revised:** 29 May 2023; **Accepted:** 01 June 2023

ABSTRACT

Extensive research has explored how Chinese herbal formulations may slow the advancement of chronic kidney disease (CKD) by modulating colonic microflora and microbiota-derived metabolites. Despite this, it remains unclear whether FuZhengHuaYuJiangZhuTongLuo (FZHY) exerts regulatory effects on CKD that parallel those reported for AST-120.To address this question, we systematically compared the influence of FZHY and AST-120 on gut microbiota composition and plasma metabolomic profiles in a chronic kidney disease model. A unilateral ureteral obstruction (UUO)-induced CKD rat model was established, after which the animals received either FZHY or AST-120. Plasma, stool, and kidney samples were subsequently evaluated using non-targeted LC-MS metabolomics, 16S rRNA sequencing, and histopathological assessment. Correlation networks linking bacterial candidates with key metabolites were also constructed. Both interventions markedly mitigated UUO-associated renal dysfunction and fibrosis while reshaping microbial communities and metabolic signatures. Relative to the untreated UUO group, FZHY administration increased the abundance of p_Firmicutes and o_Peptostreptococcales_Tissierellales, accompanied by the upregulation of 14 negative-ion and 40 positive-ion metabolites and the downregulation of 21 and 63 metabolites, respectively. In contrast, AST-120 supplementation elevated g_Prevotellaceae_NK3B31_group and f_Prevotellaceae, and altered 12 negative-ion metabolites upward and 23 downward, along with 56 positive-ion metabolites upregulated and 63 downregulated. Furthermore, FZHY enhanced bacterial biomarkers that showed negative correlations with harmful metabolites such as 4-hydroxyretinoic acid and positive correlations with beneficial ones like L-arginine. AST-120 enriched bacterial biomarkers inversely associated with toxic compounds including glycoursodeoxycholic acid, 4-ethylphenol, and indole-3-acetic acid.Both FZHY and AST-120 alleviated renal injury in the UUO-induced CKD model, potentially through restoration of disrupted microbial and metabolic pathways. Because each treatment modulated distinct bacterial taxa and metabolites, FZHY may serve as a valuable complementary therapeutic strategy alongside AST-120 in CKD management.

Keywords: Metabolism, Gut microbiota, 16S rRNA sequencing, AST-120, FuZhengHuaYuJiangZhuTongLuo recipe

How to Cite This Article: Rahman M, Karim A, Mahmud H. A Comparative Evaluation of Colonic Microflora Profiles and Plasma Metabolites in Unilateral Ureteral Obstruction–Related Chronic Kidney Disease Following Intervention with the Chinese Medicine FuZhengHuaYuJiangZhuTongLuo versus AST-120. Interdiscip Res Med Sci Spec. 2023;3(1):146-63. https://doi.org/10.51847/t1GcnyFCQ3

Introduction

Chronic kidney disease (CKD) represents a major global public health challenge, with an estimated 10 % of the adult population affected worldwide [1]. In the Asian region alone, approximately 434.3 million adults live with CKD, including 65.6 million individuals who have already progressed to its late stages [2]. CKD encompasses a range of disorders within the urinary system and typically promotes systemic inflammation alongside the retention of uremic toxins. These physiological disturbances can culminate in end-stage renal disease (ESRD),

cardiovascular complications, and other severe outcomes [3–5]. Such complications significantly contribute to mortality in advanced CKD and place substantial economic strain on healthcare systems [5, 6]. Consequently, the pursuit of cost-effective and efficient therapeutic strategies for CKD remains an urgent priority.

The gut microbial ecosystem plays essential roles in carbohydrate degradation, intestinal epithelial support, pathogen suppression, and immune and metabolic regulation. Metabolites originating from gut microorganisms—including uremic toxins, bile acids, amino acids, lipids, and organic acids—are normally cleared through renal excretion; however, their accumulation becomes harmful when kidney function declines. CKD is a multifactorial condition influenced by metabolic, endocrine, and immune dysregulation [7]. Research in CKD animal models has demonstrated elevated levels of genera such as Ruminococcus and Allobaculum [8–11], alongside increased Eggerthella lenta, Enterobacteriaceae, and Clostridium spp., with concurrent reductions in Bacteroides eggerthii, Roseburia faecis, and Prevotella spp. [1]. Microorganisms involved in butyrate production, indole biosynthesis, and mucin degradation have also been linked to CKD pathology [1]. Imbalances in gut flora not only disturb microbial composition but also drive shifts in metabolite production. For instance, harmful products such as indole and p-cresol increase in CKD, whereas beneficial metabolites—including ketone bodies—are produced in lower quantities [12]. CKD-associated metabolic disturbances further involve glycine-conjugated compounds and alterations in polyamine pathways [8]. Kidney dysfunction favors the accumulation of toxins such as indole sulfate (IS), p-cresyl sulfate (p-CS), trimethylamine, and trimethylamine-N-oxide (TMAO) [13], and failure to eliminate these metabolites accelerates CKD progression and associated comorbidities. Modulation of gut microflora has therefore emerged as a promising therapeutic avenue targeting gut–heart and gut–brain axes [14].

Interventions such as prebiotics, probiotics, and synbiotics have shown potential for restoring intestinal microecology in CKD [15]. Increasing attention has also focused on Traditional Chinese Medicine (TCM), which contains bioactive compounds capable of reshaping gut microbial communities [16–19]. The beneficial effects of TCM often arise not only from microbial transformation of its active ingredients but also from downstream alterations in functional lipid metabolites, amino acid metabolism, endotoxemia, and inflammatory cascades [20, 21]. As an alternative and complementary approach distinct from Western pharmacotherapy [22], TCM has been shown to modulate microbial profiles by elevating Firmicutes and Actinobacteria while reducing Corynebacterium and Enterococcus, and can lower circulating IS, pCS, endotoxins, and lipopolysaccharides in CKD [23].

FuZhengHuaYuJiangZhuTongLuo (FZHY) is a traditional compound formula used for antifibrotic therapy and has demonstrated activity against renal fibrosis [24]. Nonetheless, its therapeutic relevance to CKD—one of the primary clinical manifestations of renal fibrosis—remains insufficiently clarified. In this study, FZHY originates from an empirical prescription formulated by our research team according to the TCM principle of "treating from the spleen," targeting spleen–kidney Qi deficiency. Its components, which incorporate both botanical and zoological materials, are intended to harmonize meridians [25]. To characterize FZHY composition, we examined multiple TCM pharmacology databases (TCMSP, TCMID, PubChem, BATMAN-TCM), identifying 316 active constituents. Network visualization of the "drug–ingredient–target" relationships suggested strong therapeutic potential for CKD, yet the specific chemical constituents and mechanistic pathways underlying its anti-CKD actions remain unclear.

Key ingredients such as Astragalus membranaceus and Codonopsis codonopsis are known modulators of gut dysbiosis [22, 26], and they can improve immune responses, reduce serum cholesterol, and modulate T-cell activity to mitigate renal fibrosis [27]. By comparison, AST-120 is an orally administered charcoal adsorbent widely used in CKD [28]. It binds uremic toxins including IS and PCS [29, 30] and influences toxin-producing gut bacteria to improve renal outcomes [11, 31]. Despite the relevance of both therapeutics, a systematic, side-by-side evaluation of FZHY and AST-120 has not yet been reported. In the present study, we compared their effects in a unilateral ureteral obstruction (UUO)-induced CKD model, assessing microbiota composition and metabolic alterations using 16S rRNA sequencing and metabolomics. These analyses offer deeper insight into shared and divergent molecular mechanisms through which FZHY and AST-120 act to ameliorate CKD.

Materials and Methods

Preparation of FZHY

FZHY was prepared using a traditional decoction-based water extraction approach. A total of 131 g of the combined raw materials was immersed in 250 mL of water and decocted for 25–30 min. The mixture was then simmered gently for an additional 10–15 min. Two rounds of water extraction were performed using 200 mL each time, after which the combined filtrates were concentrated to 2.62 g/mL and stored at 4 °C. The formula consisted of nine botanical and zoological ingredients, and all botanical nomenclature was verified using the Kew Medicinal Plant Names Services (http://mpns.kew.org/mpns-portal/?_ga=1.111763972.1427522246.145907734).

Identification of FZHY components by UHPLC-ESI-HRMS

The FZHY extract (1.25 g/mL) was centrifuged, and the resulting supernatant was filtered through a 0.22-μm Millipore membrane. The filtrate was analyzed via UHPLC-ESI-HRMS. Chromatographic separation employed a Thermo Scientific Accucore™ C18 column (3 mm × 100 mm, 2.6 μm). The mobile phases consisted of 0.1 % formic acid in water (A) and 0.1 % formic acid in acetonitrile (B), with the following gradient: 5–50 % B over 0–30 min; 50–95 % B from 30–35 min; and 99 % B from 35–40 min. A 0.3 mL/min flow rate, 30 °C column temperature, and 3 μL injection volume were used.

Mass spectrometry was performed in both positive and negative ionization modes. Instrument settings were: spray voltage 3.2 kV, ion-source temperature 350 °C, sheath gas flow 35 arb, auxiliary gas 10 arb, and capillary temperature 320 °C. Full MS acquisition was followed by ddMS2 scanning, with a mass range of m/z 10–1000, 70,000 resolution for precursor ions, 17,500 resolution for product ions, and stepped collision energies of 20/40/60 eV.

Animals and the UUO model

Male Sprague–Dawley rats (n = 48, aged 7–8 weeks, 240–280 g) were acquired from the Laboratory Animal Business Department of the Shanghai Institute of Planned Parenthood Research (Shanghai, China). After a one-week acclimation period, the animals were randomly assigned to four experimental groups: sham (n = 12), UUO (n = 12), UUO + FZHY (n = 12), and UUO + AST-120 (n = 12).

To establish the unilateral ureteral obstruction (UUO) model, rats were anesthetized with intraperitoneal sodium pentobarbital. A left abdominal incision was made, the left ureter was exposed, and two ligatures were applied using 4–0 sutures at the middle and upper third of the ureter. The incision was then closed in anatomical layers. Sham animals underwent identical surgical handling except that ureteral ligation was omitted.

All procedures adhered to the National Institutes of Health Guidelines for the Use of Laboratory Animals and were approved by the Ethics Committee of the Hospital of Chengdu University of Traditional Chinese Medicine (approval no.: 2021DL-016). FZHY—formulated by our research group—was used as the test compound, while AST-120 served as a positive control due to its established CKD-delaying activity. FZHY was prepared following the protocol described previously [32], and administered orally at 4.92 g/kg/day [33]. AST-120 (spherical carbon adsorbent, Kureha Corporation, Japan) was delivered at 4 g/kg/day [34]. Drug administration began on the second postoperative day and continued once daily for seven consecutive days. At the time of sacrifice, seven rats from each group were selected at random and euthanized via CO_2 inhalation. Fecal samples, blood, and kidney tissues were collected for downstream analyses.

Enzyme-Linked Immunosorbent Assay (ELISA)

Blood was collected to evaluate biochemical indicators and cytokine levels. Serum was isolated by centrifugation at 3000 rpm for 20 minutes, and concentrations of serum creatinine (SCR, ml058879) and blood urea nitrogen (BUN, ml730662) were quantified using ELISA kits from Shanghai Enzyme-Linked Biotechnology Co., Ltd. (Shanghai, China).

Western blotting

Total protein was extracted from kidney tissue using RIPA lysis buffer (Sangon Biotech, Shanghai, China). Protein concentrations were quantified with a BCA assay (Beyotime, Shanghai, China). Equal amounts of protein were separated by SDS-PAGE and transferred to NC membranes. After blocking with 5% non-fat milk, membranes were incubated overnight at 4 °C with primary antibodies against α-SMA (clone 1A4, 1:1000, A2547, Sigma-Aldrich, USA) or fibronectin (clone 3E2, 1:1000, Sigma-Aldrich, USA). Following TBST washes, membranes were exposed to secondary antibodies (1:5000) for 2 h at 37 °C. Bands were visualized using enhanced

chemiluminescence (GE Healthcare Life Sciences, USA), and densitometric analysis was performed using ImageJ (version 1.4.0). GAPDH served as the loading control.

Hematoxylin & eosin and masson's trichrome staining

Kidney tissues were fixed with 4% paraformaldehyde, paraffin-embedded, and sectioned at 4 μm. Sections were processed with xylene, dehydrated in graded ethanol, and stained with H&E or Masson's trichrome (Sigma-Aldrich; Merck KGaA). After staining and ethanol dehydration (70% and 90%), six random microscopic fields per sample (400× magnification) were examined using an Olympus optical microscope (Tokyo, Japan) to assess renal injury and fibrosis.

DNA extraction and 16S rRNA sequencing

Genomic DNA was isolated from fecal samples using the SDS extraction method. DNA purity and concentration were evaluated using a multimode microplate reader (BioTek Instruments, Inc.). The V4–V5 region of the 16S rRNA gene was amplified with primers 16S-F (5′-GTGCCAGCMGCCGCGG-3′) and 16S-R (5′-CCGTCAATTMTTTRAGTTT-3′). PCR reactions were performed using Phusion® High-Fidelity PCR Master Mix with GC buffer. Amplicons were purified with the GeneJET Gel Extraction Kit (Thermo Scientific), used to construct a TruSeq® DNA PCR-Free library, and sequenced on a NovaSeq6000 platform (Novogene Bioinformatics Technology, Beijing, China).

16S rRNA data processing

Raw sequencing reads generated from NovaSeq PE250 were subjected to quality control with Trimmomatic (version 0.36). Operational Taxonomic Units (OTUs) were clustered at 97% sequence similarity using UPARSE (version 7.0.1001). Taxonomic assignments were conducted using the Mothur workflow and the SILVA138 SSU rRNA database. MUSCLE (version 3.8.31) was applied to align representative OTU sequences and infer phylogenetic relationships.

Alpha-diversity indices (Shannon, Simpson) were calculated via QIIME (version 1.9.1), and group differences were evaluated by t-tests. Principal Coordinate Analysis (PCoA) was performed using the vegan package in R (version 3.6.0). Differentially abundant taxa were identified with LEfSe analysis.

Metabolomics

Untargeted liquid chromatography–mass spectrometry (LC-MS) profiling of plasma metabolites was conducted as described previously [35]. Data processing, peak alignment, and metabolite identification were performed using Compound Discoverer 3.1. Data normalization and log-transformation were done using MetaX [36].

Differential metabolites were selected using PLS-DA with the following thresholds:

- VIP > 1.0
- FoldChange > 1.5 or < 0.667
- $P < 0.05$ [37]

Volcano plots were used for visualization. Associations between altered genera and metabolites were assessed with Spearman's correlation (significance defined as $|R| > 0.4$ and $P < 0.05$).

Statistical analysis

GraphPad Prism 8.0 (GraphPad Software, San Diego, USA) was used for all computations. Data are displayed as mean ± standard deviation (SD). Differences among groups were assessed using one-way ANOVA, followed by Tukey's post hoc comparison. Statistical significance was defined as $P < 0.05$, with $^{*}P < 0.05$ and $^{**}P < 0.01$ marking graded significance levels.

Results and Discussion

Chemical composition of FZHY

FZHY was dissolved in methyl alcohol and examined by UHPLC-ESI-HRMS, which yielded a catalogue of 115 detectable constituents. These components encompassed multiple chemical families: 11 amino acids, 10 flavonoids, eight organic acids, seven alkaloids, six purine derivatives, five volatile oils, four glycosides, and four

salvianolic acids. Additional compounds were rare (fewer than two per class) or grouped under "Other". According to the Traditional Chinese Medicine Systems Pharmacology Database and Analysis Platform (https://old.tcmsp-e.com/tcmsp.php), several well-recognized therapeutic constituents were present in FZHY, including danshensu, hydroxysafflor yellow A, ononin, baicalin, salvianolic acid B, scutellarin methylester, calycosin, chrysophanol-8-O-β-D-glucopyranoside, wogonoside, wogonin, rhein, and skullcapflavone II.

Administering either FZHY or AST-120 improved the kidney function of UUO model rats

To determine whether the two treatments could counteract CKD progression, renal functional markers and morphological alterations were examined in rats subjected to unilateral ureteral obstruction. ELISA revealed markedly elevated serum SCR and BUN in the UUO group compared with sham-operated controls **(Figures 1a and 1b)**. Western blotting confirmed that α-SMA and Fibronectin levels were likewise increased in the UUO kidneys **(Figure 1c)**. Histological staining (H&E and Masson's trichrome) showed pronounced pathological features, including dilation of renal tubules, inflammatory infiltration, and extensive fibrosis **(Figures 1d and 1e)**. Administration of FZHY or AST-120 mitigated these disruptions, yielding lower SCR and BUN values, reduced α-SMA and Fibronectin expression, and visibly less structural injury in renal tissues **(Figures 1a–1e).**

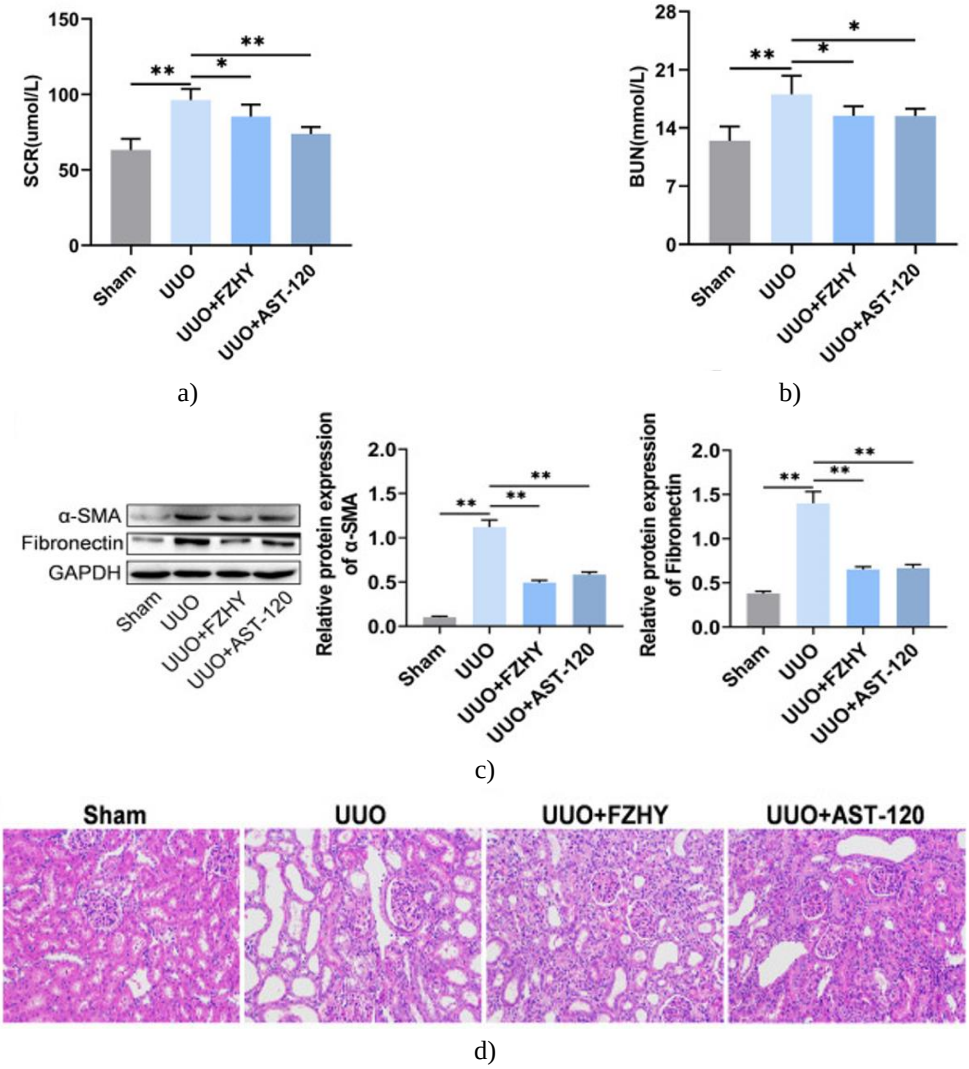

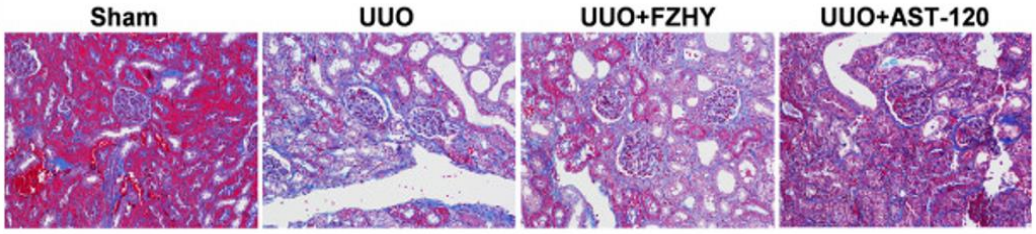

e)

Figure 1. Multiple indicators of renal injury.

(a) Serum creatinine (SCR) levels are compared among rats in the sham, UUO, UUO + FZHY, and UUO + AST-120 groups.

(b) Blood urea nitrogen (BUN) concentrations are shown for the same four groups.

(c) Western blotting displays the expression of α-SMA and Fibronectin in renal tissues from each experimental group.

(d) Microscopic evaluation of kidney damage using H&E staining (400×) in all groups.

(e) Renal fibrosis visualized by Masson's trichrome staining (400×).

Statistical significance: *P < 0.05, **P < 0.01.

Administering FZHY or AST-120 influenced the intestinal flora of the UUO model rats

Given that both treatments alleviated renal injury by day 7, we next explored whether these interventions also shaped gut microbial patterns by performing 16S rRNA sequencing on fecal samples from all groups. To assess how FZHY or AST-120 affected microbial communities, α-diversity measures (richness and diversity) were compared among the UUO, UUO + FZHY, and UUO + AST-120 groups. The Shannon and Simpson indices decreased significantly following FZHY treatment relative to UUO, whereas AST-120 caused a mild increase in both indices **(Figures 2a and 2b).**

Beta-diversity analysis (weighted distance) further revealed clear separation among the microbial communities of the three groups, indicating distinct shifts in overall composition **(Figure 2c).**

LEfSe analysis was then used to pinpoint microbial taxa that contributed most strongly to the observed differences. Numerous bacterial groups differed between the UUO and treatment groups. In rats receiving FZHY, taxa enriched relative to UUO included p_Firmicutes, o_Peptostreptococcales_Tissierellales, f_Peptostreptococcale, s_Romboutsia, o_Clostridiales, f_Clostridiaceae, g_Clostridium_sensu_stricto_1, o_Erysipelotrichales, f_Erysipelotrichaceae, g_Turicibacter, c_Gammaproteobacteria, and p_Proteobacteria. Conversely, the UUO group showed higher abundances of o_Clostridia_UCG_014, o_Oscillospirales, f_Lachnospiraceae, o_Lachnospirales, f_Muribaculaceae, p_Bacteroidota, c_Bacteroidia, and o_Bacteroidales.

Comparison of the UUO and UUO + AST-120 groups indicated that g_Prevotellaceae_NK3B31_group and f_Prevotellaceae were elevated after AST-120 administration. In contrast, o_Lactobacillales, f_Lactobacillaceae, g_Lactobacillus, f_Muribaculaceae, s_Lactobacillus_johnsonii, and s_Lactobacillus_reuteri were more abundant in the untreated UUO group **(Figures 2d and 2e).**

Notably, f_Muribaculaceae was the only taxonomic group showing changes in response to both FZHY and AST-120 in the UUO model.

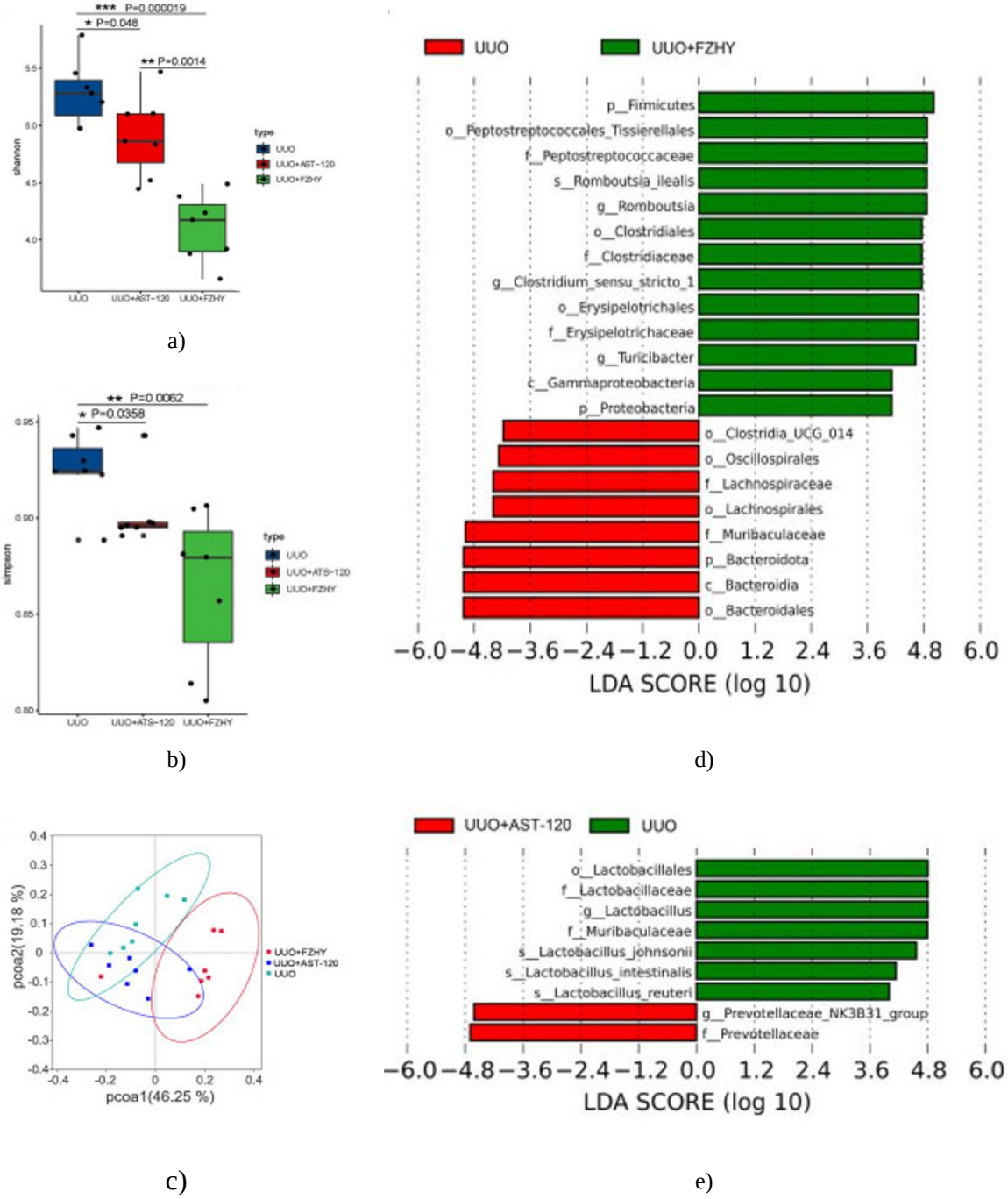

Figure 2. Differentially abundant microbiota across taxonomic levels

Shifts in microbial richness and diversity were assessed through α-diversity measurements using the Shannon (a) and Simpson (b) indices derived from OTU abundance in the UUO, UUO + FZHY, and UUO + AST-120 groups. Variation in overall community structure was examined through a PCoA plot based on UniFrac distances (c). LEfSe-based linear discriminant analysis, accompanied by cladogram visualization, identified key taxa that distinguished the UUO group from the UUO + FZHY group (d) and from the UUO + AST-120 group (e). Taxa shown in red indicate enrichment in the red-labelled group, whereas green bars denote taxa comparatively enriched in the green-labelled group. Significance levels are represented as *P < 0.05, **P < 0.01, and ***P < 0.001. Taxonomic abbreviations: p (phylum), c (class), o (order), f (family), g (genus), s (species). For color interpretation, refer to the online article.

Administering FZHY or AST-120 improved dysregulated plasma metabolites in UUO model rats

To explore how each treatment modulates metabolic pathways, an untargeted LC-MS metabolomic analysis was conducted on plasma samples, using both positive and negative ion detection modes**.**

Principal component analyses revealed clear separations between the metabolic profiles of UUO rats and those treated with either FZHY or AST-120 in both ion modes **(Figures 3a, 3b, 4a and 4b).**

Volcano plot comparisons showed that, relative to the UUO group, the FZHY-treated rats exhibited 14 elevated and 21 reduced metabolites in the negative ion mode, whereas AST-120 produced 12 elevated and 23 reduced metabolites **(Figures 3c and 3d)**. For the positive ion mode, 40 metabolites increased and 63 decreased after FZHY administration, and 56 increased and 63 decreased with AST-120 treatment **(Figures 4c and 4d).**

PLS-DA Z-score analyses identified 30 discriminative cationic and anionic metabolites distinguishing the UUO + FZHY and UUO groups, as well as the UUO + AST-120 and UUO groups **(Figures 3e, 3f, 4e and 4f).**

KEGG enrichment analysis of anionic metabolites revealed that the FZHY-associated differences mapped predominantly to Steroid hormone biosynthesis, Arachidonic acid metabolism, and Amoebiasis pathways, totaling 22 enriched pathways. In contrast, the AST-120-related anionic changes were grouped into 11 pathways, notably Thiamine metabolism, Terpenoid backbone biosynthesis, and Dopaminergic synapse pathways **(Figures 3g and 3h).**

The two treatments shared enriched pathways involving Steroid hormone biosynthesis, Dopaminergic synapse, and Tyrosine metabolism.

In the positive ion analyses, FZHY-associated metabolites mapped to 15 pathways, primarily Oxidative phosphorylation and Steroid hormone biosynthesis. AST-120 altered 20 pathways, with major enrichment in Cortisol synthesis and secretion and Cushing's syndrome pathways **(Figures 4g and 4h).**

Shared cation-related enrichments between both treatments included Oxidative phosphorylation, Steroid hormone biosynthesis, 2-Oxocarboxylic acid metabolism, Riboflavin metabolism, Mineral absorption, Drug metabolism–cytochrome P450, Phenylalanine/tyrosine/tryptophan biosynthesis, Protein digestion and absorption, Amino acid biosynthesis, Unsaturated fatty acid biosynthesis, Phenylalanine metabolism, Aminoacyl-tRNA biosynthesis, Neuroactive ligand–receptor interaction, and ABC transporters.

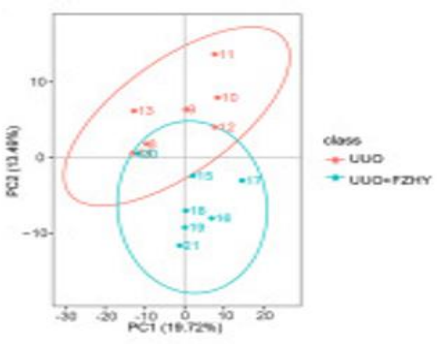

a)

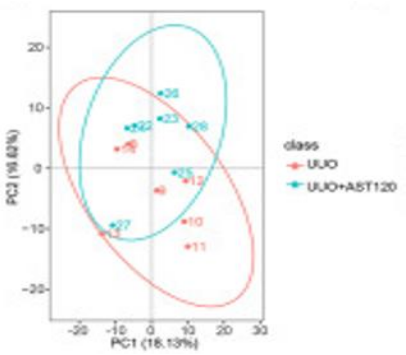

b)

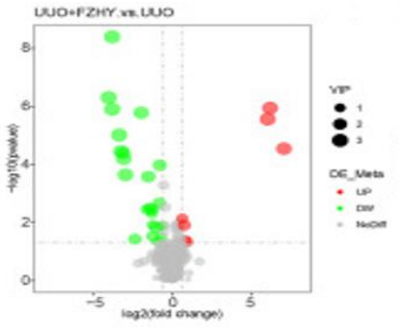

c)

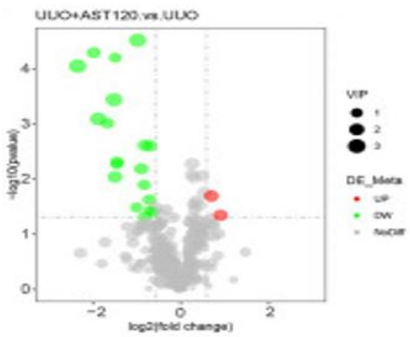

d)

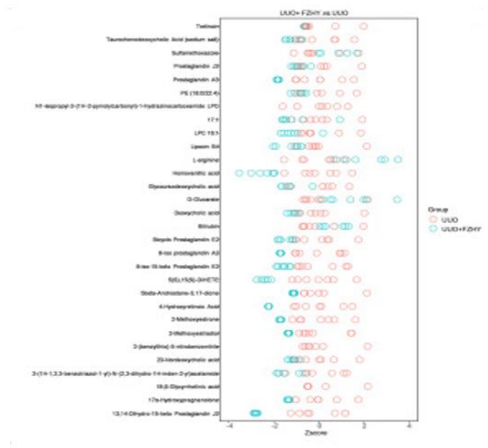

e)

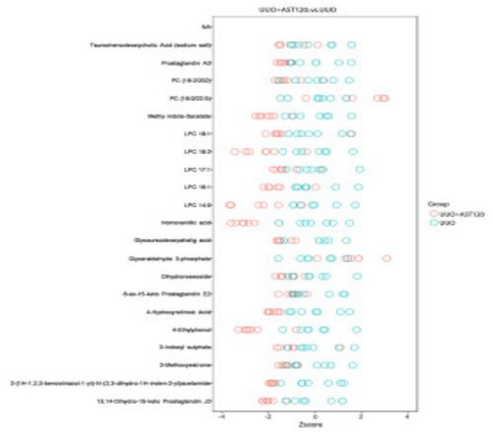

f)

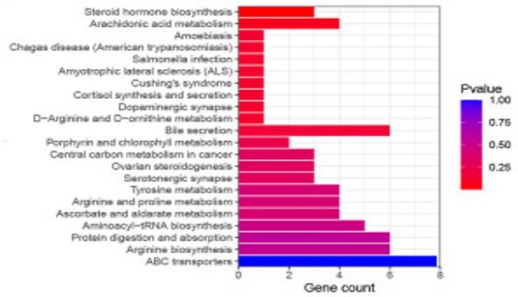

g)

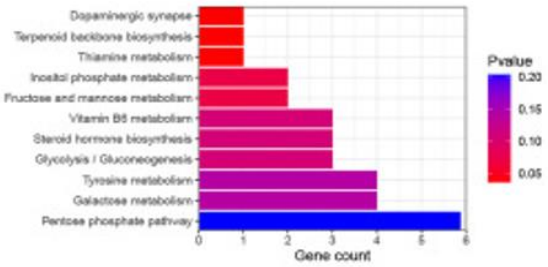

h)

Figure 3. Analysis of cationic metabolites by metabolomics

Partial least squares discriminant analysis (PLS-DA) was used to evaluate overall changes in metabolite profiles, comparing UUO rats with those treated with FZHY (a) and with AST-120 (b). Volcano plots were generated to highlight significantly altered metabolites between UUO and UUO + FZHY (c) as well as UUO and UUO + AST-120 (d). Z-score transformations were applied to illustrate the relative abundance shifts of metabolites in the UUO versus UUO + FZHY groups (e) and UUO versus UUO + AST-120 groups (f). Furthermore, KEGG pathway enrichment was performed on the metabolites showing the most pronounced differences under negative ion mode to identify impacted metabolic pathways in UUO + FZHY versus UUO (g) and UUO + AST-120 versus UUO (h).

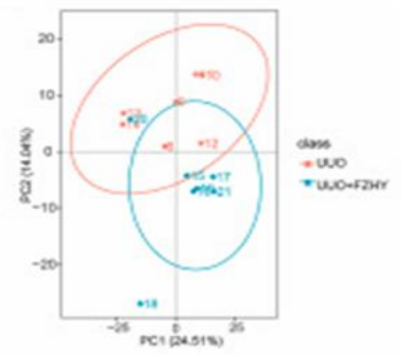

a)

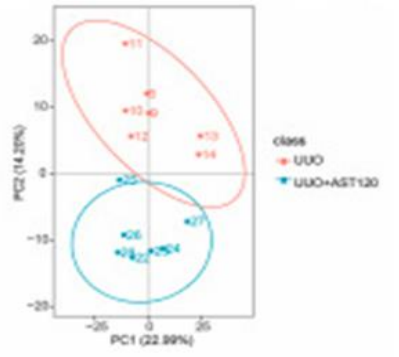

b)

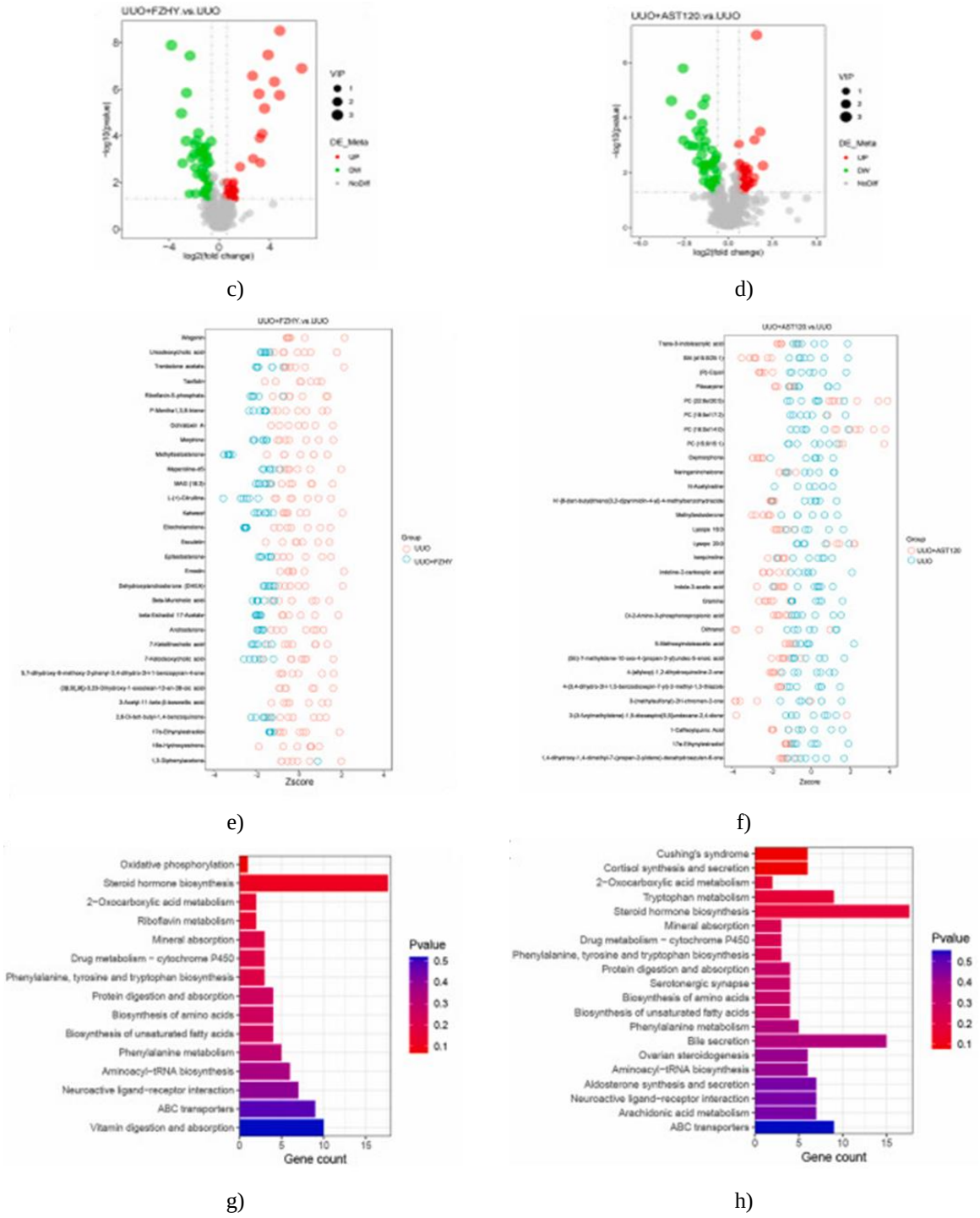

Figure 4. Metabolomics of negatively charged metabolites

To explore changes in plasma anionic metabolites, PLS-DA was used to visualize global metabolite patterns between the UUO group and the UUO + FZHY group (a) as well as the UUO and UUO + AST-120 group (b). Volcano plots highlighted metabolites that were significantly up- or down-regulated in UUO + FZHY versus UUO (c) and UUO + AST-120 versus UUO (d). Relative abundance changes were further represented using Z-scores for UUO + FZHY (e) and UUO + AST-120 (f) compared with UUO. Pathway enrichment analysis based on KEGG databases identified the main metabolic pathways affected by these anionic metabolites for UUO + FZHY (g) and UUO + AST-120 (h), with results displayed under positive ion mode.

Linking gut microbiota alterations to plasma metabolites

To determine how shifts in gut microbiota relate to plasma metabolites, Pearson correlation analysis was conducted. For the UUO + FZHY group versus UUO, correlations were assessed between 21 bacterial biomarkers and the top 20 positive and 20 negative ion metabolites. FZHY-induced microbial changes were associated with metabolites such as amino acids, bile acids, and other organic compounds, including citrulline, 23-nordeoxycholic acid, and homovanillic acid **(Figures 5a and 5b).**

For the UUO + AST-120 group versus UUO, nine microbial biomarkers were correlated with the most altered positive and negative metabolites, showing links to bile acids, phenols, and organic acids like glycoursodeoxycholic acid, 3-indoxyl sulfate, and 4-ethylphenol **(Figures 6a and 6b).**

Across both treatments, ten metabolites—including cholic acid, androstane steroids, and other organic compounds—were commonly associated with microbial shifts. In the FZHY group, all ten metabolites showed strong positive correlations with f_Muribaculaceae, whereas in the AST-120 group, only five metabolites—homovanillic acid, 4-hydroxyretinoic acid, 13,14-dihydro-15-keto prostaglandin J2, taurochenodeoxycholic acid (sodium salt), and methyltestosterone—remained significantly correlated with f_Muribaculaceae.

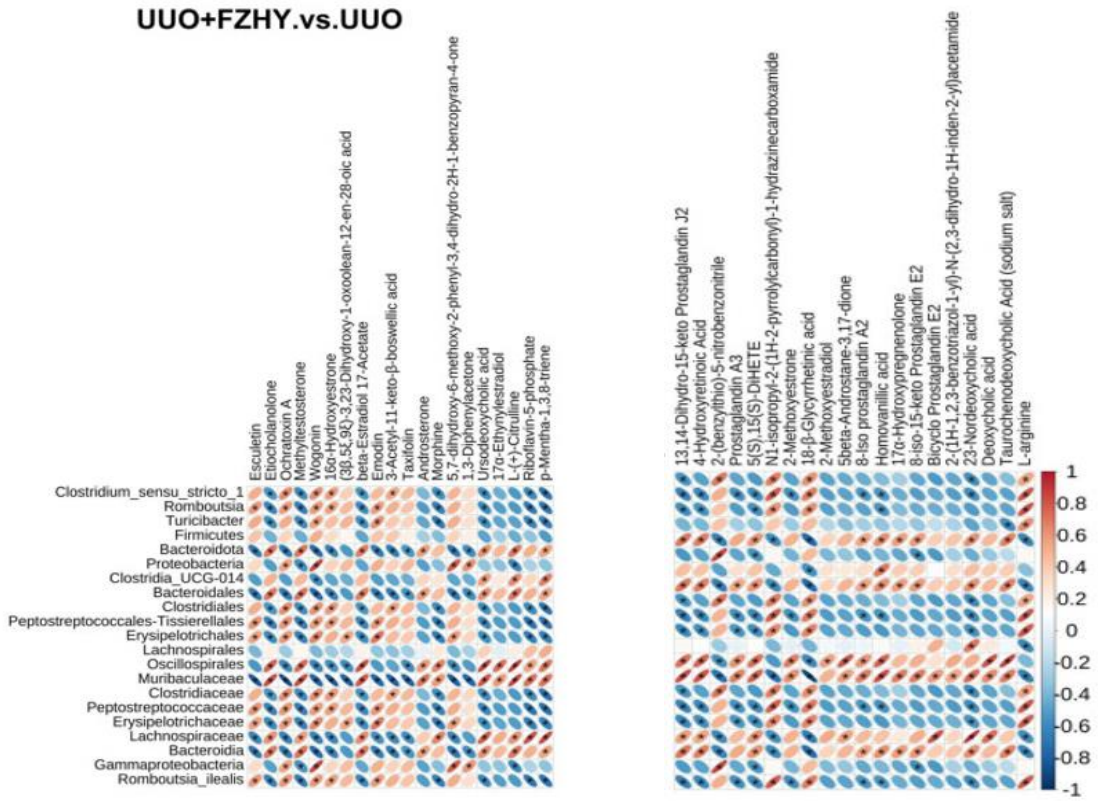

a) b)

Figure 5. Correlation analysis for UUO + FZHY treatment

Correlation relationships between altered gut microbiota and plasma metabolites were examined in the UUO + FZHY group relative to UUO. A heatmap displays the associations between the differential bacterial taxa and the top 20 positive ion metabolites (a). Another heatmap illustrates the correlations between the differential microbiota and the top 20 negative ion metabolites (b). Strong positive or negative relationships are indicated by the intensity of the colors in the heatmap.

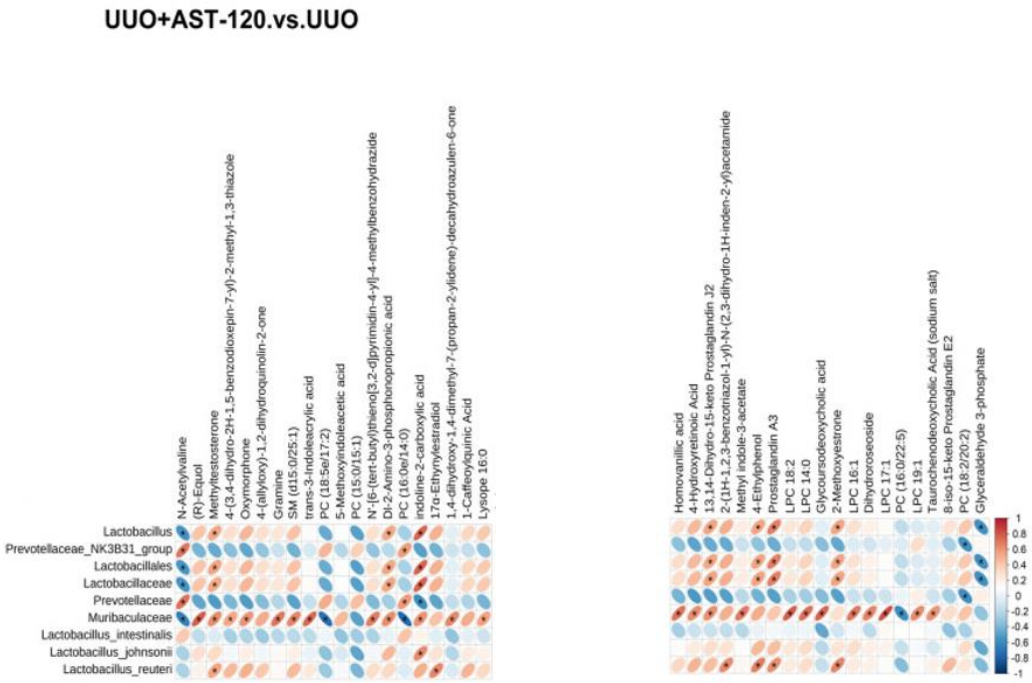

a) b)

Figure 6. Correlation analysis for UUO + AST-120 treatment

The relationships between altered gut microbiota and plasma metabolites were assessed in the UUO + AST-120 group relative to UUO. A heatmap demonstrates the correlations between the differential bacterial taxa and the top 20 positive ion metabolites (a), while another heatmap shows the associations with the top 20 negative ion metabolites (b). The intensity and color gradient reflect the strength and direction of the correlations.

Recent studies have explored the impact of gut microbiota on clinical outcomes in CKD and compared traditional Chinese medicine (TCM) formulations with conventional kidney-targeted drugs. For example, the TCM Jian-Pi-Yi-Shen (JPYS) decoction demonstrated superior therapeutic effects over piperazine ferulate in improving renal outcomes [22]. Active components of TCM can reach the colon and modulate the intestinal microbiota and its metabolites, potentially contributing to CKD management. In our investigation, FZHY treatment promoted renal function recovery and mitigated fibrosis in UUO rats, displaying efficacy comparable to AST-120, though the patterns of microbiota and metabolite responses differed markedly between the two treatments.

CKD is frequently accompanied by mild systemic inflammation, gut dysbiosis, and compromised intestinal barrier function [38]. Previous research indicates that AST-120 can partially reverse gut microbial imbalances in CKD patients [11]. In our study, AST-120 treatment reduced the abundance of Lactobacillus species while increasing g_Prevotellaceae_NK3B31_group and f_Prevotellaceae, consistent with previous observations linking Lactobacillus abundance to CKD severity markers such as plasma tryptophan levels [39, 40]. Prevotellaceae_UCG_001 NK3B31_group exhibits anti-inflammatory properties and negatively correlates with IL-6 and TNF-α [41]. Butyrate-producing members of f_Prevotellaceae, which are reduced in CKD patients, help maintain intestinal barrier integrity and modulate inflammation [42]. These findings confirm that AST-120 effectively ameliorates gut microbial dysbiosis in CKD.

FZHY administration also significantly altered the intestinal microbiota of UUO rats. Studies have suggested that the Firmicutes/Bacteroidetes (F/B) ratio is associated with various diseases, including CKD [43, 44], although some reports indicate minimal changes in CKD patients [39]. In our study, FZHY increased p_Firmicutes and decreased p_Bacteroidota in UUO rats, highlighting potential microbiota-modulating effects. The abundance of o_Clostridiales, which differs significantly between CKD patients and healthy individuals, may act as a probiotic to support kidney function [45]. Short-chain fatty acid-producing bacteria such as g_Clostridium_sensu_stricto_1 enhance intestinal barrier integrity and may facilitate CKD recovery [46]. Other taxa, including o_Erysipelotrichales, exert renal protective effects and may slow CKD progression [47]. g_Turicibacter has

demonstrated anti-inflammatory activity, and reductions in g_Turicibacter and g_Clostridium correlate with decreased tryptophan, lysine, and propionic acid levels, promoting tubulointerstitial fibrosis in CKD [40, 48]. Elevated abundances of c_Gammaproteobacteria and p_Proteobacteria are characteristic of CKD [49]. However, the roles of s_Romboutsia and o_Oscillospirales in CKD remain unclear, warranting further investigation.

Imbalances in gut microbiota in CKD rats are closely linked to alterations in plasma metabolites. In this study, LC-MS analysis of kidney and plasma samples revealed that FZHY treatment significantly reduced the levels of metabolites such as 4-hydroxyretinoic acid, 5(S),15(S)-DiHETE, 23-nordeoxycholic acid, deoxycholic acid, ursodeoxycholic acid, taurochenodeoxycholic acid (sodium salt), and citrulline, while elevating L-arginine levels. These compounds are primarily involved in the metabolism of prenol lipids, phenolic compounds, fatty acyls, bile acids, and amino acids. Elevated hydroxyretinoic acid is a recognized marker of chronic nephritis [50], and plasma homovanillic acid levels closely reflect renal clearance function [51]. The inflammatory mediator 5(S),15(S)-DiHETE, derived from leukocytes, is typically increased in CKD and correlates with inflammatory status [52]. Bile acids, metabolites generated by gut bacteria, tend to accumulate in the serum of CKD patients and animal models [53]. Administration of FZHY decreased the concentrations of 23-nordeoxycholic acid, deoxycholic acid, ursodeoxycholic acid, and taurochenodeoxycholic acid, thereby mitigating CKD-related damage, consistent with previous reports [54].

Additionally, plasma citrulline levels are higher in early-stage CKD [55], whereas L-arginine supplementation promotes NO and urea synthesis, supporting detoxification and renal protection [56, 57]. These findings collectively suggest that FZHY can lower harmful metabolites and contribute to CKD recovery in UUO rats. Correlation analysis revealed that in FZHY-treated UUO rats, the relative abundance of p_Firmicutes, o_Clostridiales, g_Clostridium_sensu_stricto_1, o_Erysipelotrichales, and g_Turicibacter negatively correlated with bile acids, 5(S),15(S)-DiHETE, and citrulline, while positively correlating with L-arginine. In contrast, p_Bacteroidota showed an inverse association pattern.

AST-120 treatment yielded similar metabolic effects, including reductions in homovanillic acid, 4-hydroxyretinoic acid, and taurochenodeoxycholic acid. It also decreased levels of glycoursodeoxycholic acid, 4-ethylphenol, methyl indole-3-acetate, 3-indoxyl sulfate, indoline-2-carboxylic acid, 5-methoxyindoleacetic acid, and indole-3-acetic acid, which are involved in bile acid and indole metabolism. Dysregulated bile acid and toxin metabolism can exacerbate CKD, as supported by prior studies [53, 58, 59]. Correlation analysis indicated that Lactobacillus abundance positively correlated with toxins such as 4-ethylphenol and indoline-2-carboxylic acid, while g_Prevotellaceae_NK3B31_group and f_Prevotellaceae showed no significant associations with these compounds. Both FZHY and AST-120 decreased Muribaculaceae abundance, a bacterial group involved in complex carbohydrate degradation and positively associated with harmful metabolites such as ursodeoxycholic acid, citrulline, 4-hydroxyretinoic acid, homovanillic acid, methyl indole-3-acetate, and indoline-2-carboxylic acid, suggesting its potential role in CKD regulation.

KEGG pathway analysis further revealed that differential metabolites in both UUO + FZHY and UUO + AST-120 groups were enriched in steroid hormone biosynthesis and amino acid metabolism, including tyrosine and phenylalanine. Steroids, including vitamin D, are typically deficient in CKD patients [60]. Vitamin D contributes to renal protection, reduces inflammation, downregulates the renin-angiotensin system, prevents epithelial-to-mesenchymal transition, and regulates parathyroid hormone levels [61]. Uremic retention solutes such as indoxyl sulfate (IS) and p-cresyl sulfate (pCS), generated from tryptophan, phenylalanine, and tyrosine by gut microbes, accumulate in CKD and drive disease progression [63, 63]. Enhanced metabolism of these amino acids increases p-cresol production, a precursor of uremic toxins that impairs renal function [64].

Overall, these findings indicate that both FZHY and AST-120 may alleviate renal injury by restoring metabolite homeostasis, a process likely mediated through the gut microbiota. However, their mechanisms differ: AST-120 acts as a charcoal adsorbent that directly removes uremic toxins such as IS from the kidney, indirectly leading to secondary renoprotective effects including microbiota and metabolite rebalancing. Conversely, FZHY contains multiple bioactive compounds that not only reduce harmful metabolites in the intestine and suppress their production but also directly attenuate tubulointerstitial fibrosis [65].

To explore the relationship between the primary chemical constituents of FZHY that were relatively abundant and gut microbiota, we reviewed the relevant literature. Hydroxysafflor yellow A has been reported to increase the relative abundance of the genus Romboutsia and reduce the Firmicutes/Bacteroidetes (F/B) ratio [66]. In cases of intestinal dysbiosis caused by disease, baicalin can restore beneficial bacteria by elevating p_Firmicutes levels

while reducing the increase in p_Proteobacteria, thereby helping to reestablish microbial balance [67, 68]. Salvianolic acid B similarly increases p_Firmicutes and decreases p_Proteobacteria [69]. Currently, there is no literature on the effects of scutellarin methylester or wogonoside on gut microbiota, nor on their potential associations with f_Muribaculaceae, which is influenced by both FZHY and AST-120.

Regarding kidney-related effects, baicalin has demonstrated renoprotective activity by suppressing NF-κB-mediated inflammatory pathways [70, 71], whereas hydroxysafflor yellow A mitigates renal fibrosis through inhibition of TGF-β1-induced epithelial-to-mesenchymal transition (EMT) [72]. Salvianolic acid B also modulates TGF-β1 signaling and EMT or Nrf2 pathways to protect against kidney fibrosis or ischemia/reperfusion injury [73, 74]. While the roles of scutellarin methylester and wogonoside in kidney disease remain insufficiently characterized, the deglycosylated form of wogonoside, mogonin—a key FZHY monomer—has been shown to exert renoprotective effects [75, 76]. These findings suggest that FZHY contains multiple bioactive components capable of protecting renal function via modulation of gut microbiota. Nevertheless, the interactions among these monomers, the microbiota, and anti-CKD effects are complex and require further investigation.

Previous studies on individual active components of FZHY and their influence on plasma metabolites in CKD are limited, and in some cases, their findings are not fully consistent with ours. This supports the idea that the therapeutic effects of FZHY likely arise from the synergistic action of multiple components rather than a single compound [77, 78]. Taken together, our results and prior research indicate that the main active molecules in FZHY significantly modulate both CKD progression and gut microbiota composition, though each component may exert distinct or even contrasting effects when administered alone or in combination.

Conclusion

In summary, this study demonstrated that both FZHY and AST-120 alleviate renal injury and fibrosis. While both treatments influence gut microbiota and plasma metabolites, the mechanisms by which they act differ, as evidenced by distinct microbial and metabolic profiles. Our findings suggest that FZHY could potentially serve as a complementary therapy for CKD patients receiving AST-120. However, further research is necessary to elucidate the specific anti-fibrotic effects of FZHY's principal active compounds.

Acknowledgments: The language of this study was professionally edited by ExEditing.com

Conflict of Interest: None

Financial Support: This study was supported by National Natural Science Foundation of China (Nos.: 81,973,673 and 82,274,487 to Ming Chen) and Science and Technology Foundation of Sichuan Province (No.: 2021YFS0034 to Ming Chen).

Ethics Statement: None

References

1. Lohia S, Vlahou A, Zoidakis J, Smith P, Brown T, Wilson K. Microbiome in chronic kidney disease (CKD): an omics perspective. Toxins. 2022;14(3).
2. Liyanage T, Toyama T, Hockham C, Ninomiya T, Perkovic V, Woodward M. Prevalence of chronic kidney disease in Asia: a systematic review and analysis. BMJ Glob Health. 2022;7(1).
3. Aron-Wisnewsky J, Clément K, Smith P, Brown T, Wilson K, Harris J. The gut microbiome, diet, and links to cardiometabolic and chronic disorders. Nat Rev Nephrol. 2016;12(3):169-81.
4. Sampaio-Maia B, Simões-Silva L, Pestana M, Araujo R, Soares-Silva IJ, Smith P. The role of the gut microbiome on chronic kidney disease. Adv Appl Microbiol. 2016;96:65-94.
5. GBD Chronic Kidney Disease Collaboration, Smith P, Brown T, Wilson K, Harris J, Clark R. Global, regional, and national burden of chronic kidney disease, 1990-2017: a systematic analysis for the global burden of disease study 2017. Lancet. 2020;395(10225):709-33.

6. Mantovani A, Zusi C, Smith P, Brown T, Wilson K, Harris J. PNPLA3 gene and kidney disease. Explor Med. 2020;1:42-50.
7. Zoccali C, Vanholder R, Massy ZA, Ortiz A, Sarafidis P, Dekker FW. The systemic nature of CKD. Nat Rev Nephrol. 2017;13(6):344-58.
8. Feng YL, Cao G, Chen DQ, Vaziri ND, Chen L, Zhang J. Microbiome-metabolomics reveals gut microbiota associated with glycine-conjugated metabolites and polyamine metabolism in chronic kidney disease. Cell Mol Life Sci. 2019;76(24):4961-78.
9. Mishima E, Fukuda S, Shima H, Hirayama A, Akiyama Y, Takeuchi Y. Alteration of the intestinal environment by lubiprostone is associated with amelioration of adenine-induced CKD. J Am Soc Nephrol. 2015;26(8):1787-94.
10. Zeng YQ, Dai Z, Lu F, Lu Z, Liu X, Chen C. Emodin via colonic irrigation modulates gut microbiota and reduces uremic toxins in rats with chronic kidney disease. Oncotarget. 2016;7(14):17468-78.
11. Kikuchi M, Ueno M, Itoh Y, Suda W, Hattori M, Smith P. Uremic toxin-producing gut microbiota in rats with chronic kidney disease. Nephron. 2017;135(1):51-60.
12. Poesen R, Windey K, Neven E, Kuypers D, De Preter V, Augustijns P. The influence of CKD on colonic microbial metabolism. J Am Soc Nephrol. 2016;27(5):1389-99.
13. Coppo R, Smith P, Brown T, Wilson K, Harris J, Clark R. The gut-kidney axis in IgA nephropathy: role of microbiota and diet on genetic predisposition. Pediatr Nephrol. 2018;33(1):53-61.
14. Cosola C, Rocchetti MT, Sabatino A, Fiaccadori E, Di Iorio BR, Gesualdo L. Microbiota issue in CKD: how promising are gut-targeted approaches? J Nephrol. 2019;32(1):27-37.
15. Chauveau P, Aparicio M, Bellizzi V, Campbell K, Hong X, Johansson L. Mediterranean diet as the diet of choice for patients with chronic kidney disease. Nephrol Dial Transplant. 2018;33(5):725-35.
16. Huang L, Luo X, Chen M, Smith P, Brown T, Wilson K. Effects and safety of traditional Chinese medicine on the gut microbiota of an adult with chronic kidney disease: a protocol for systematic review and meta-analysis. Medicine (Baltimore). 2022;101(7):e28847.
17. Jia Q, Wang L, Zhang X, Ding Y, Li H, Yang Y. Prevention and treatment of chronic heart failure through traditional Chinese medicine: role of the gut microbiota. Pharmacol Res. 2020;151:104552.
18. Feng W, Ao H, Peng C, Yan D, Smith P, Brown T. Gut microbiota, a new frontier to understand traditional Chinese medicines. Pharmacol Res. 2019;142:176-91.
19. Zhang W, Miikeda A, Zuckerman J, Jia X, Charugundla S, Zhou Z. Inhibition of microbiota-dependent TMAO production attenuates chronic kidney disease in mice. Sci Rep. 2021;11(1):518.
20. Lin TL, Lu CC, Lai WF, Wu TS, Lu JJ, Chen YM. Role of gut microbiota in identification of novel TCM-derived active metabolites. Protein Cell. 2021;12(5):394-410.
21. Zhang HY, Tian JX, Lian FM, Li M, Liu WK, Zhen Z. Therapeutic mechanisms of traditional Chinese medicine to improve metabolic diseases via the gut microbiota. Biomed Pharmacother. 2021;133:110857.
22. Zheng L, Chen S, Wang F, Huang S, Liu X, Yang X. Distinct responses of gut microbiota to Yian-si-ni-Shen decoction are associated with improved clinical outcomes in 5/6 nephrectomized rats. Front Pharmacol. 2020;11:604.
23. Zhao T, Zhang H, Yin X, Zhao H, Ma L, Yan M. Tangshen formula modulates gut microbiota and reduces gut-derived toxins in diabetic nephropathy rats. Biomed Pharmacother. 2020;129:110325.
24. Li H, Smith P, Brown T, Wilson K, Harris J, Clark R. Advances in anti-hepatic fibrotic therapy with traditional Chinese medicine herbal formula. J Ethnopharmacol. 2020;251:112442.
25. Chen FZ, You LJ, Yang F, Wang LN, Guo XQ, Gao F. CNGBdb: China national genebank database. Yi Chuan. 2020;42(8):799-809.
26. Zou J, Li W, Wang G, Fang S, Cai J, Wang T. Hepatoprotective effects of Huangqi decoction (Astragali Radix and Glycyrrhizae Radix et Rhizoma) on cholestatic liver injury in mice: involvement of alleviating intestinal microbiota dysbiosis. J Ethnopharmacol. 2021;267:113544.
27. Xi Y, Lu X, Zhu L, Sun X, Jiang Y, He W. Clinical trial for conventional medicine integrated with traditional Chinese medicine (TCM) in the treatment of patients with chronic kidney disease. Medicine (Baltimore). 2020;99(21):e20234.

28. Yoshifuji A, Wakino S, Irie J, Matsui A, Hasegawa K, Tokuyama H. Oral adsorbent AST-120 ameliorates gut environment and protects against the progression of renal impairment in CKD rats. Clin Exp Nephrol. 2018;22(5):1069-78.
29. Sato E, Saigusa D, Mishima E, Uchida T, Miura D, Morikawa-Ichinose T. Impact of the oral adsorbent AST-120 on organ-specific accumulation of uremic toxins: LC-MS/MS and MS imaging techniques. Toxins. 2017;10(1).
30. Edwards D. High risk groups for chlamydial infection. N Z Med J. 1988;101(842):151-2.
31. Sato E, Hosomi K, Sekimoto A, Mishima E, Oe Y, Saigusa D. Effects of the oral adsorbent AST-120 on fecal p-cresol and indole levels and on the gut microbiota composition. Biochem Biophys Res Commun. 2020;525(3):773-9.
32. Chen Z, Chen M, He K, Chen Y, Smith P, Brown T. Exploration of TCM syndrome in the animal model of 5/6 nephrectomy and prescription syndrome test of Tuzheng Huayu Jiangzhuo Kongluo prescription. Chin J Basic Med Tradit Chin Med. 2021;27(11):5.
33. Qin T, Wu L, Qian H, Song Z, Pan Y, Liu T. Prediction of the mechanisms of action of Shenkang in chronic kidney disease: a network pharmacology study and experimental validation. J Ethnopharmacol. 2020;246:112128.
34. Vaziri ND, Yuan J, Khazaeli M, Masuda Y, Ichii H, Liu S. Oral activated charcoal adsorbent (AST-120) ameliorates chronic kidney disease-induced intestinal epithelial barrier disruption. Am J Nephrol. 2013;37(6):518-25.
35. Dunn WB, Broadhurst D, Begley P, Zelena E, Francis-McIntyre S, Anderson N. Procedures for large-scale metabolic profiling of serum and plasma using gas chromatography and liquid chromatography coupled to mass spectrometry. Nat Protoc. 2011;6(7):1060-83.
36. Wen B, Mei Z, Zeng C, Liu S, Smith P, Brown T. metaX: a flexible and comprehensive software for processing metabolomics data. BMC Bioinformatics. 2017;18(1):183.
37. Heischmann S, Quinn K, Cruickshank-Quinn C, Liang LP, Reisdorph R, Reisdorph N. Exploratory metabolomics profiling in the kainic acid rat model reveals depletion of 25-hydroxyvitamin D3 during epileptogenesis. Sci Rep. 2016;6:31424.
38. Vaziri ND, Zhao YY, Pahl MV, Smith P, Brown T, Wilson K. Altered intestinal microbial flora and impaired epithelial barrier structure and function in CKD: the nature, mechanisms, consequences and potential treatment. Nephrol Dial Transplant. 2016;31(5):737-46.
39. Li F, Wang M, Wang J, Li R, Zhang Y, Smith P. Alterations to the gut microbiota and their correlation with inflammatory factors in chronic kidney disease. Front Cell Infect Microbiol. 2019;9:206.
40. Chen L, Chen DQ, Liu JR, Zhang J, Vaziri ND, Zhuang S. Unilateral ureteral obstruction causes gut microbial dysbiosis and metabolome disorders contributing to tubulointerstitial fibrosis. Exp Mol Med. 2019;51(3):1-18.
41. Wei X, Tao J, Xiao S, Jiang S, Shang E, Zhu Z. Xiexin Tang improves the symptom of type 2 diabetic rats by modulation of the gut microbiota. Sci Rep. 2018;8(1):3685.
42. Hu J, Zhong X, Yan J, Zhou D, Qin D, Xiao X. High-throughput sequencing analysis of intestinal flora changes in ESRD and CKD patients. BMC Nephrol. 2020;21(1):12.
43. Sumida K, Kovesdy CP, Smith P, Brown T, Wilson K, Harris J. The gut-kidney-heart axis in chronic kidney disease. Physiol Int. 2019;106(3):195-206.
44. Pahl MV, Vaziri ND, Smith P, Brown T, Wilson K, Harris J. The chronic kidney disease-colonic axis. Semin Dial. 2015;28(5):459-63.
45. Wu R, Ruan XL, Ruan DD, Zhang JH, Wang HL, Zeng QZ. Differences in gut microbiota structure in patients with stages 4-5 chronic kidney disease. Am J Transl Res. 2021;13(9):10056-74.
46. Wlodarska M, Willing BP, Bravo DM, Finlay BB, Smith P, Brown T. Phytonutrient diet supplementation promotes beneficial Clostridia species and intestinal mucus secretion resulting in protection against enteric infection. Sci Rep. 2015;5:9253.
47. Tu Y, Fang QJ, Sun W, Liu BH, Liu YL, Wu W. Total flavones of Abelmoschus manihot remodel gut microbiota and inhibit microinflammation in chronic renal failure progression by targeting autophagy-mediated macrophage polarization. Front Pharmacol. 2020;11:566611.

48. Rausch P, Steck N, Suwandi A, Seidel JA, Künzel S, Bhullar K. Expression of the blood-group-related gene B4galnt2 alters susceptibility to Salmonella infection. PLoS Pathog. 2015;11(7):e1005008.
49. Chen YY, Chen DQ, Chen L, Liu JR, Vaziri ND, Guo Y. Microbiome-metabolome reveals the contribution of gut-kidney axis on kidney disease. J Transl Med. 2019;17(1):5.
50. Han KH, Kim B, Ji SC, Kang HG, Cheong HI, Cho JY. Mechanism of chronic kidney disease progression and novel biomarkers: a metabolomic analysis of experimental glomerulonephritis. Metabolites. 2020;10(4).
51. Potter WZ, Hsiao JK, Goldman SM, Smith P, Brown T, Wilson K. Effects of renal clearance on plasma concentrations of homovanillic acid: methodologic cautions. Arch Gen Psychiatry. 1989;46(6):558-62.
52. Chavis C, Chanez P, Vachier I, Bousquet J, Michel FB, Godard P. 5-15-diHETE and lipoxins generated by neutrophils from endogenous arachidonic acid as asthma biomarkers. Biochem Biophys Res Commun. 1995;207(1):273-9.
53. Wang X, Yang S, Li S, Zhao L, Hao Y, Qin J. Aberrant gut microbiota alters host metabolome and impacts renal failure in humans and rodents. Gut. 2020;69(12):2131-42.
54. Jovanovich A, Isakova T, Block G, Stubbs J, Smits G, Chonchol M. Deoxycholic acid, a metabolite of circulating bile acids, and coronary artery vascular calcification in CKD. Am J Kidney Dis. 2018;71(1):27-34.
55. Duranton F, Lundin U, Gayrard N, Mischak H, Aparicio M, Mourad G. Plasma and urinary amino acid metabolomic profiling in patients with different levels of kidney function. Clin J Am Soc Nephrol. 2014;9(1):37-45.
56. Baylis C. Nitric oxide deficiency in chronic kidney disease. Am J Physiol Renal Physiol. 2008;294(1):F1-9.
57. Klahr S, Morrissey J. L-arginine as a therapeutic tool in kidney disease. Semin Nephrol. 2004;24(4):389-94.
58. Kobayashi T, Matsumura Y, Ozawa T, Yanai H, Iwasawa A, Kamachi T. Exploration of novel predictive markers in rat plasma of the early stages of chronic renal failure. Anal Bioanal Chem. 2014;406(5):1365-76.
59. Shen B, Pardi DS, Bennett AE, Queener E, Kammer P, Hammel JP. The efficacy and tolerability of AST-120 (spherical carbon adsorbent) in active pouchitis. Am J Gastroenterol. 2009;104(6):1468-74.
60. Jean G, Souberbielle JC, Chazot C, Smith P, Brown T, Wilson K. Vitamin D in chronic kidney disease and dialysis patients. Nutrients. 2017;9(4).
61. Panizo S, Martínez-Arias L, Alonso-Montes C, Cannata P, Martín-Carro B, Fernández-Martín JL. Fibrosis in chronic kidney disease: pathogenesis and consequences. Int J Mol Sci. 2021;22(1).
62. Liu J, Yue S, Yang Z, Feng W, Meng X, Wang A. Oral hydroxysafflor yellow A reduces obesity in mice by modulating the gut microbiota and serum metabolism. Pharmacol Res. 2018;134:40-50.
63. Aronov PA, Luo FJ, Plummer NS, Quan Z, Holmes S, Hostetter TH. Colonic contribution to uremic solutes. J Am Soc Nephrol. 2011;22(9):1769-76.
64. Gryp T, Vanholder R, Vaneechoutte M, Glorieux G, Smith P, Brown T. p-Cresyl sulfate. Toxins. 2017;9(2).
65. Chen Z, Wu S, Zeng Y, Chen Z, Li X, Li J. FuZhengHuaYuJiangZhuTongLuoFang prescription modulates gut microbiota and gut-derived metabolites in UUO rats. Front Cell Infect Microbiol. 2022;12:837205.
66. Liu Y, Li J, Yu J, Wang Y, Lu J, Shang EX. Disorder of gut amino acids metabolism during CKD progression is related with gut microbiota dysbiosis and metagenome change. J Pharm Biomed Anal. 2018;149:425-35.
67. Zhu L, Xu LZ, Zhao S, Shen ZF, Shen H, Zhan LB. Protective effect of baicalin on the regulation of Treg/Th17 balance, gut microbiota and short-chain fatty acids in rats with ulcerative colitis. Appl Microbiol Biotechnol. 2020;104(12):5449-60.
68. Liu J, Zhang T, Wang Y, Si C, Wang X, Wang RT. Baicalin ameliorates neuropathology in repeated cerebral ischemia-reperfusion injury model mice by remodeling the gut microbiota. Aging (Albany NY). 2020;12(4):3791.

69. Bai Y, Bao X, Mu Q, Fang X, Zhu R, Liu C. Ginsenoside Rb1, salvianolic acid B and their combination modulate gut microbiota and improve glucolipid metabolism in high-fat diet induced obese mice. PeerJ. 2021;9:e10598.
70. Wang K, Feng C, Li C, Yao J, Xie X, Gong L. Baicalin protects mice from aristolochic acid I-induced kidney injury by induction of CYP1A through the aromatic hydrocarbon receptor. Int J Mol Sci. 2015;16(7):16454-68.
71. Liao S, Pei L, Wang J, Zhang Q, Xu D, Yang M. Protection of baicalin against lipopolysaccharide induced liver and kidney injuries based on 1H NMR metabolomic profiling. Toxicol Res. 2016;5(4):1148-59.
72. Hu N, Duan J, Li H, Wang Y, Wang F, Chu J. Hydroxysafflor yellow A ameliorates renal fibrosis by suppressing TGF-β1-induced epithelial-to-mesenchymal transition. PLoS One. 2016;11(4):e0153409.
73. Wang QL, Tao YY, Yuan JL, Shen L, Liu CH, Smith P. Salvianolic acid B prevents epithelial-to-mesenchymal transition through the TGF-β1 signal transduction pathway in vivo and in vitro. BMC Cell Biol. 2010;11(1):1-16.
74. Pang Y, Zhang PC, Lu RR, Li HL, Li JC, Fu HX. Salvianolic acid B modulates caspase-1-mediated pyroptosis in renal ischemia-reperfusion injury via Nrf2 pathway. Front Pharmacol. 2020;11:541426.
75. Meng XM, Li HD, Wu WF, Tang PMK, Ren GL, Gao L. Wogonin protects against cisplatin-induced acute kidney injury by targeting RIPK1-mediated necroptosis. Lab Invest. 2018;98(1):79-94.
76. Lei L, Zhao J, Liu XQ, Chen J, Qi XM, Xia LL. Wogonin alleviates kidney tubular epithelial injury in diabetic nephropathy by inhibiting PI3K/Akt/NF-κB signaling pathways. Drug Des Devel Ther. 2021;15:3131.
77. Song Y, Hu T, Gao H, Zhai J, Gong J, Zhang Y. Altered metabolic profiles and biomarkers associated with astragaloside IV-mediated protection against cisplatin-induced acute kidney injury in rats: an HPLC-TOF/MS-based untargeted metabolomics study. Biochem Pharmacol. 2021;183:114299.
78. Liu X, Zhang B, Huang S, Wang F, Zheng L, Lu J. Metabolomics analysis reveals the protection mechanism of Huangqi-Danshen decoction on adenine-induced chronic kidney disease in rats. Front Pharmacol. 2019;10:992.